Magnetite biomineralization in *Magnetospirillum magneticum* is regulated by a switch-like behavior in the HtrA protease MamE

David M. Hershey[1], Patrick J. Browne[1], Anthony T. Iavarone[2,3], Joan Teyra[4], Eun H. Lee[5], Sachdev S. Sidhu[4], and Arash Komeili[1,2,5]*

[1] *Department of Plant and Microbial Biology, University of California, Berkeley, CA 94720, USA*
[2] *California Institute for Quantitative Biosciences, University of California, Berkeley, CA 94720, USA*
[3] *QB3/Chemistry Mass Spectrometry Facility, University of California, Berkeley, CA 94720, USA*
[4] *Department of Molecular Genetics, Terrance Donnelly Centre for Cellular and Biomedical Research, University of Toronto, Toronto, Canada ON M5S 3E1*
[5] *Department of Molecular and Cell Biology, University of California, Berkeley, CA 94720, USA*

Running title: Reconstituting MamE-dependent proteolysis

To whom correspondence should be addressed: Prof. Arash Komeili, Department of Plant and Microbial Biology, University of California – Berkeley, 261 Koshland Hall, Berkeley, California 94720, email: komeili@berkeley.edu.

Keywords: Magnetosome, biomineralization, serine protease, bacterial genetics, allosteric regulation, microbiology, magnetite, magnetotactic bacteria

Abstract: Magnetotactic bacteria are aquatic organisms that produce subcellular magnetic crystals in order to orient in the earth's geomagnetic field. The genetic basis for this process has been dissected in the model magnetotactic bacterium *Magnetospirillum magneticum* AMB-1, leading to the identification of biomineralization genes that control the formation and growth of magnetite crystals. One such factor, MamE, is a predicted member of the HtrA family of serine proteases, a widespread enzyme family that plays important roles in protein turnover and quality control. MamE was recently shown to promote the proteolytic processing of itself and two other biomineralization factors *in vivo*. Here, we have studied MamE-dependent proteolysis in detail. We analyzed the *in vivo* processing patterns of three proteolytic targets and used this information to reconstitute proteolysis with a purified form of MamE. MamE cleaves a custom peptide substrate with positive cooperativity, and its auto-proteolysis can be stimulated with exogenous substrates or peptides that bind to either of its PDZ domains. A constitutively active form of the protease causes biomineralization defects, showing that proper regulation of its activity is required during biomineralization *in vivo*. Our results demonstrate for the first time that MamE is a bonafide HtrA protease and that its activity is consistent with the previously proposed checkpoint model for biomineralization.

Introduction: Interactions between living organisms and insoluble inorganic compounds are an underexplored aspect of biology. Magnetotactic bacteria assemble magnetic crystals called magnetosomes into chains within their cells allowing them to passively align and navigate along magnetic fields(1, 2). Genetic analyses have shown that magnetosome formation is a complex developmental process controlled by a conserved set of genes(3-7). A subset of these, called biomineralization factors, whose deletions disrupt or eliminate magnetite crystal formation, have drawn increasing interest for their potential utility in biomedical applications(8). Understanding the biochemical mechanisms employed by these gene products can provide novel strategies for manipulating transition metal-based nanomaterials *in vitro*(9-11).

Two predicted trypsin-like proteases, MamE and MamO, are required to produce magnetite in the model magnetotactic organism, *Magnetospirillum magneticum* AMB-1(3). Disrupting either gene abolishes the formation of magnetite crystals without affecting the development of their surrounding membrane

compartment, indicating that both proteins are required for magnetite nucleation within the magnetosome lumen(3, 12, 13). Furthermore, deleting *mamE* causes a number of proteins that normally localize at the magnetosomes to become dispersed throughout the cytoplasmic membrane. Adding either wild-type or catalytically inactive (E^{PD}) alleles of *mamE* complements the protein localization defect, but only the wild-type allele restores normal magnetite biosynthesis(14).

Cells with the E^{PD} allele show an intermediate biomineralization phenotype in which they produce small magnetite particles. While wild-type AMB-1 has a distribution of crystal sizes centered at 50-60nm in diameter, the size distribution in the E^{PD} cells is centered at ~20nm. Interestingly, ~97% of the crystals in the E^{PD} strain are smaller than 35nm, the point above which magnetite particles become paramagnetic and can hold a stable magnetic dipole. The correlation between mineral sizes in the E^{PD} strain and the superparamagnetic to paramagnetic transition point lead to the speculation that MamE's putative protease activity regulates the transition to a magnetotactic lifestyle. This so-called checkpoint model predicts that cells produce small superparamagnetic crystals until an unknown signal activates MamE, promoting maturation to paramagnetic particles(14).

MamE is a member of the HtrA/DegP family of trypsin-like proteases, a ubiquitous family of enzymes that controls various aspects of protein quality control(15). The family is characterized by domain structures consisting of an N-terminal trypsin-like domain and one or two C-terminal postsynaptic density 95/discs large/zonula occludens-1 (PDZ) domains(16-18). Like many proteases, intricate regulatory mechanisms are a hallmark of HtrA catalysis(19, 20). Based on structural and mechanistic investigations, the PDZ domains play several roles in regulating proteolysis including promoting assembly and activating the protease domain by binding to extended peptide motifs(21-24). MamE has an unusual domain structure in which a tandem *c*-type cytochrome motif has been inserted between the protease and two PDZ domains (Fig. 1A)(14). Unfortunately, studies aimed at understanding the catalytic activity of MamE and its regulation have been hindered by an inability to obtain recombinant protein.

Recently, MamE was found to promote the *in vivo* proteolytic processing of itself, MamO, and another biomineralization factor named MamP in a manner that required the predicted MamE active site(25-27). Although MamO was also required for these proteolytic events, this effect did not require the predicted MamO active site. Subsequent structural analysis showed that MamO's protease domain was locked in an inactive state and incapable of catalysis, suggesting that it played a non-catalytic role in activating MamE(25). Despite the genetic evidence for MamE's role in proteolysis, its activity has not been confirmed directly using purified components. Here, we have characterized MamE-dependent proteolysis in detail and identified a number of regulatory mechanisms. Developing a method to purify MamE and analyzing *in vivo* proteolytic patterns of each target facilitated reconstitution of MamE-dependent proteolysis *in vitro*. Detailed analysis of its catalytic activity suggests a switch-like model in which the basal state of the protein is an inactive form that can be turned on through a number of routes. A constitutively active allele of MamE disrupts biomineralization, confirming that properly regulated proteolysis is critical to magnetosome formation.

Experimental procedures:

Strains, plasmids and growth conditions

The strains and plasmids used in this study are described in Table 1 and Table 2, respectively. AMB-1 was maintained in MG medium supplemented with kanamycin when necessary as previously described (3). Magnetic response was measured using the coefficient of magnetism as previously described (3). Standard molecular biology techniques were used for plasmid manipulation. *E. coli* strains were grown in LB medium supplemented with appropriate antibiotics. Plasmids were maintained in *E. coli* strain DH5α *λpir*. *E. coli* strain WM3064 was used for plasmid conjugations as described previously(3).

Immunoblotting

Whole-cell lysates of AMB-1 strains were prepared from 10mL cultures and analyzed as described previously(25). For analysis of the auto-cleavage reaction products, a 1 in 10 dilution of

each time-point was separated on a 12% acrylamide gel for immunoblotting. The MamE and MamP antibodies have been described previously(25). The anti-6xHis (Sigma), anti-FLAG (Sigma), anti-σ70 (Thermo Fisher) and anti-strep (Qiagen) antibodies were purchased from commercial sources.

Fractionation of MamO fragments

A strain with the genetic background Δ*O*Δ*R9*/*FLAG-O* was cultured without shaking at 30 °C in 2 L screw-capped flasks that were filled to the top with MG medium. The cells were harvested by spinning at 5k x g for 15 min, re-suspending in cold 20mL 25mM Tris-HCl pH7.4, re-spinning at 8k x g for 10 min and freezing the resulting pellet at -80°C until use. Cell pellets were thawed on ice and re-suspended in 5mL lysis buffer A (10mM Tris-HCl pH 8.0, 50mM NaCl, 1mM EDTA). Pepstatin A and leupeptin were added to a final concentration of 2μg/mL and PMSF was added to 2mM. Lysozyme was added from 50mg/mL stock to a final concentration of 0.5mg/mL and the cells were incubated at room temperature for 15 min. 15mL of lysis buffer B (20mM HEPES-KOH pH7.5, 50mM NaCl, 1.25mM $CaCl_2$) was added along with DTT to 2mM and DNAse to 5μg/mL and the suspension was incubated for 15min at 4°C with agitation. The cells were sonicated twice for 10 seconds and the suspension was spun at 8k x g for 10min to isolate the magnetite-associated material.

The resulting pellet was re-suspended in 5.5 mL solubilization buffer (20mM BisTris-HCl pH7.0, 75mM NaCl, 10% glycerol) and CHAPS was added to 1% from a 10% stock solution. The suspension was incubated at room temperature for 15min with agitation followed by an incubation for 15min at 4°C with agitation. The suspension was spun at 16k x g for 15min. The resulting pellet was re-suspended in 5.5 mL solubilization buffer and the detergent extraction was repeated with 1% FosCholine. The FosCholine-soluble material was loaded on a 1mL HiTrap Q FF column (GE Healthcare) that had been equilibrated with solubilization buffer containing 0.03% *n*-dodecyl β-D-maltoside (DDM). The column was washed with 10mL of solubilization buffer with 0.03% DDM and eluted with 4mL of buffer Q1 (20mM BisTris-HCl pH7.0, 275mM NaCl, 10% glycerol) with 0.03% DDM followed by 4mL of buffer Q2 (20mM BisTris-HCl pH7.0, 400mM NaCl, 10% glycerol) with 0.03% DDM. The Q1 fraction was added to 50μL anti-FLAG M2 resin (Sigma) and incubated at 4°C with agitation for 3 hrs. The resin was isolated by spinning at 4k x g and washed with sequential 1mL washes of buffer Q2, buffer Q1 and solubilization buffer each containing 0.03% DDM. Bound proteins were eluted by 3 washes with 50μL of 0.2M glycine pH 2.8, which were pooled with 50μL of 1M Tris-HCl pH8.0.

Preparation of trypsin digests for liquid chromatography-mass spectrometry (LC-MS)

The concentrated FLAG elution fraction was separated on a 12% acrylamide gel and stained with colloidal Coomassie Blue. A ~3 x 10mm section of the gel corresponding to the processed MamO band was excised from the gel and chopped into small pieces. These were washed with 100mM NH_4HCO_3 followed by reduction and alkylation of cysteines with DTT and iodoacetamide. The gel pieces were then dehydrated by washing with increasing concentrations of acetonitrile in 100mM NH_4HCO_3 and dried under vacuum. A 0.1mg/mL solution of trypsin was used to re-swell the gel pieces, and they were incubated overnight at 37°C. The resulting peptides were extracted from the gel slices with successive washes of 0.1% formic acid solutions containing increasing concentrations of acetonitrile. The extracts were pooled in a fresh tube, concentrated under vacuum to remove the organic phase and stored at 4°C until analysis.

LC-MS

Trypsin-digested protein samples were analyzed using a Thermo Dionex UltiMate3000 RSLCnano liquid chromatograph that was connected in-line with an LTQ-Orbitrap-XL mass spectrometer equipped with a nanoelectrospray ionization (nanoESI) source (Thermo Fisher Scientific, Waltham, MA). The LC was equipped with a C18 analytical column (Acclaim® PepMap RSLC, 150 mm length × 0.075 mm inner diameter, 2 μm particles, 100 Å pores, Thermo) and a 1-μL sample loop. Acetonitrile (Fisher Optima grade, 99.9%), formic acid (1-mL ampules, 99+%, Thermo Pierce), and water purified to a resistivity of 18.2 MΩ·cm (at 25 °C) using a Milli-Q Gradient ultrapure water purification system (Millipore, Billerica, MA) were used to prepare

mobile phase solvents. Solvent A was 99.9% water/0.1% formic acid and solvent B was 99.9% acetonitrile/0.1% formic acid (v/v). The elution program consisted of isocratic flow at 2% B for 4 min, a linear gradient to 30% B over 38 min, isocratic flow at 95% B for 6 min, and isocratic flow at 2% B for 12 min, at a flow rate of 300 nL/min.

Full-scan mass spectra were acquired in the positive ion mode over the range m/z = 350 to 1800 using the Orbitrap mass analyzer, in profile format, with a mass resolution setting of 60,000 (at m/z = 400, measured at full width at half-maximum peak height, FWHM), which provided isotopic resolution for singly and multiply charged peptide ions. Thus, an ion's mass and charge could be determined independently, i.e., the charge state was determined from the reciprocal of the spacing between adjacent isotope peaks in the m/z spectrum. In the data-dependent mode, the eight most intense ions exceeding an intensity threshold of 50,000 counts were selected from each full-scan mass spectrum for tandem mass spectrometry (MS/MS) analysis using collision-induced dissociation (CID). MS/MS spectra were acquired using the linear ion trap, in centroid format, with the following parameters: isolation width 3 m/z units, normalized collision energy 30%, default charge state 3+, activation Q 0.25, and activation time 30 ms. Real-time charge state screening was enabled to exclude unassigned and 1+ charge states from MS/MS analysis. Real-time dynamic exclusion was enabled to preclude re-selection of previously analyzed precursor ions, with the following parameters: repeat count 2, repeat duration 10 s, exclusion list size 500, exclusion duration 90 s, and exclusion mass width 20 ppm. Data acquisition was controlled using Xcalibur software (version 2.0.7, Thermo). Raw data were searched against the *Magnetospirillum magneticum* AMB-1 FASTA protein database using Proteome Discoverer software (version 1.3, SEQUEST algorithm, Thermo). Peptide identifications were validated by manual inspection of MS/MS spectra, i.e., to check for the presence of y-type and b-type fragment ions[1] that identify the peptide sequences(28).

Expression and purification of MamE

pAK825 or pAK964 was transferred to C43 cells (Lucigen) that had been previously transformed with the pEC86 heme-loading plasmid(29). The transformed cells were maintained at 30°C due to toxicity of the construct at 37°C. An overnight liquid culture was inoculated into 600mL 2xYT medium supplemented with the appropriate antibiotics. The cultures were grown at 30°C until the OD_{600} reached ~0.5, at which point the culture was transferred to 20°C. After a 30 min equilibration, the culture was induced with 35µM IPTG. Expression was performed for 12.5-13 hrs at 20°C with shaking at 200 rpm.

Cells were harvested by immediately chilling the cultures on ice and spinning at 6k x g for 10 min. The resulting pellet was re-suspended in 50mL of cold osmotic shock buffer (50mM NaPhosphate pH8.0, 1mM EDTA, 20% sucrose). Leupeptin (1.5µg/mL), pepstatin A (1.5µg/mL) and lysozyme (0.5mg/mL) were added, and the suspension was rocked at room temperature for 15 min. An equal volume of ice-cold H_2O was added and the suspension was rocked on ice for 15 min before spinning at 8k x g for 10 min to remove debris.

The resulting supernatant was added to 3 mL Ni-NTA resin (Qiagen) and supplemented with NaCl (150mM), DNAseI (5µg/mL), NP-40 (0.1%) and $MgCl_2$ (2.5mM). The slurry was rocked at 4°C for 30 min and the beads were allowed to settle. After decanting the upper phase, the slurry was poured into a column, washed with 10 column volumes of Ni wash buffer (25mM Tris-HCl pH7.4, 250mM NaCl, 10mM imidazole, 10% glycerol) and the bound proteins eluted with Ni elution buffer (25mM Tris-HCl pH7.4, 250mM NaCl, 250mM imidazole, 10% glycerol). The Ni-NTA eluent was loaded onto a 1mL StrepTrap column (GE Healthcare), which was then washed with 5mL strep wash buffer (25mM Tris-HCl pH7.4, 250mM NaCl, 10% glycerol). Bound proteins were eluted in strep wash buffer containing 2.5mM desthiobiotin. The purified protein was concentrated in 50kDa cutoff ultrafilter while simultaneously removing the desthiobiotin by repeated dilution and concentration with strep wash buffer. The concentration was determined by the Bradford method using bovine serum albumin to prepare a standard curve. Aliquots were frozen in liquid N_2 and stored at -80°C until use.

Analysis of MamO1 peptide cleavage

A custom peptide with the sequence 5-carboxymethylfluorescein-Thr-Gln-Thr-Val-Ala-Ala-Gly-Ser-Lys(CPQ2)-D-Arg-D-Arg was obtained commercially (CPC Scientific). The peptide was dissolved in DMSO and stored at -20°C. 5X substrate solutions with various concentrations of the MamO1 peptide were prepared in assay buffer (50mM Tris-HCl pH8.0) containing 0.05% NP-40 and 1.6% DMSO. To initiate the reaction, 10µL samples of the substrate mix were added to 40µL of MamE protein solution that had been diluted to 125nM in assay buffer in a 96-well plate. The fluorescence was scanned (excitation: 485nm; emission 538nm) every 5 min for 2 hrs in a Tecan plate reader.

The slope was determined from the linear portion of each reaction. Cleavage rates were calculated by making a standard curve from a MamO1 cleavage reaction that had been incubated for 24hrs to allow for complete hydrolysis. Specific activities were determined by normalizing these cleavage rates to the enzyme concentration. Rates were plotted as a function of peptide concentration and fit to the Hill form of the Michaelis-Menten equation using the Kaleidagraph software package:

$$V = \frac{V_{max}[\mathrm{O1}]^n}{{K_m}^n + [\mathrm{O1}]^n}$$

Analysis of MamE auto-proteolysis

25µL reactions were prepared by adding 1µL of activating peptide dissolved in DMSO at the appropriate concentration to 24µL of MamE diluted to 2µM in assay buffer. The reactions were incubated at 30°C, and 8µL aliquots were removed at the appropriate times. Each aliquot was quenched immediately by mixing with SDS sample buffer. Equal volumes of each aliquot were separated on a 12% acrylamide SDS-PAGE gel and stained with Coomassie Blue to visualize the processing pattern.

Expression and purification of PDZ domains

For all three PDZ domain constructs (EP1, EP2 and EP12), the appropriate plasmids for expression as N-terminal 6xHis-MBP-TEV fusions were transformed into BL21 Codon Plus cells. Cultures were grown in 2xYT at 37°C until the OD_{600} reached ~0.8 at which point they were transferred to 20°C for 30min followed by induction with 0.1mM IPTG and expression overnight. The cells were harvested by centrifugation, resuspended in resuspension buffer (25mM Tris-HCl pH7.4, 800mM NaCl, 10mM imidazole, 10% glycerol) and frozen at -80°C until use.

For protein purification, the cells were thawed on ice and sonicated for three 30-second cycles. The lysate was clarified by spinning at 13k x g for 30 min. The resulting supernatant was loaded on a 3mL Ni-NTA column that had been equilibrated in resuspension buffer. After washing with 10 column volumes of resuspension buffer and 10 column volumes of wash buffer 2 (25mM Tris-HCl pH7.4, 400mM NaCl, 25mM imidazole, 10% glycerol), bound proteins were eluted with Ni elution buffer.

For the purification of the EP1 and EP2 proteins, the elution fractions were dialyzed overnight against AEX buffer A (25mM BisTris-HCl pH7.0, 75mM NaCl and 10% glycerol). The desalted protein was passed through a 1mL HiTrap QFF column (GE Healthcare) and the flow-through was concentrated in a 50kDa cutoff ultrafilter, injected onto a16/60 Superdex 200 column and developed in Storage Buffer. Each protein eluted as a single symmetrical peak. The peak fractions were concentrated in a 50kDa ultrafilter and small aliquots were frozen in liquid N_2 and stored at -80°C for use in the phage display experiments.

For the purification of the EP12 protein, the elution fraction was dialyzed overnight against digest buffer (50mM NaPhosphate pH8.0, 75mM NaCl, 5mM imidazole, 10% glycerol) in the presence of 6xHis tagged TEV protease to remove the 6xHis-MBP tag. The resulting sample was passed through a 3mL Ni-NTA column that had been equilibrated in digest buffer. The flow-through fraction was concentrated in a 10kDa ultrafilter, passed through a 1mL HiTrap SP FF column and concentrated again before injection on a16/60 Superdex 200 column that was developed in storage buffer. The protein eluted as a single symmetrical peak. The peak fractions were concentrated in a 10kDa ultrafilter and small aliquots were frozen in liquid N_2 and stored at -80°C for use in the fluorescence anisotropy experiments.

Phage display

C-terminally and N-terminally displayed peptide libraries were used to assess the peptide binding preferences of MamE PDZ1 and PDZ2. The C-terminal peptide library consisted of random decapeptides constructed using 10 consecutive NNK degenerate codons encoding for all 20 natural amino acids and fused to the C terminus of a mutant M13 bacteriophage major coat protein (2×10^{10} unique members)(8, 30). The N-terminal peptide library consisted of random hexadecapeptides constructed using 16 consecutive mixes of 19 codon trimers (cysteine and STOP codons were excluded) and fused to the N terminus phage coat protein (2.4×10^{11} unique members)(31).

The phage display selections followed an established protocol used previously for the PDZ human domains(32, 33). Briefly, each library was separately cycled through rounds of binding selection against each immobilized MBP-PDZ fusion protein on 96-well MaxiSorp immunoplates (Nalge Nunc). After each round, phage were propagated in *E. coli* XL1-blue cells (Stratagene) supplemented with M13-KO7 helper phage (New England Biolabs) to facilitate phage production. After four rounds of selection, phages from individual clones were analyzed in a phage enzyme-linked immunosorbent assay (ELISA). Phages that bound to the MBP-PDZ fusion but not a control MBP were subjected to DNA sequence analysis.

Fluorescence anisotropy

Peptides with the following sequences were synthesized commercially with a fluorescein-aminocaproic acid group fused to the N-terminus: WSQEMEDWFWQMPLSG (PDZ1*) and MEDYGIFMTSPEGPWA (PDZ2*). Each peptide was diluted to a concentration of 40nM in 25mM Tris-HCl pH7.4 containing 0.25mg/mL bovine serine albumin. A dilution series of EP12 protein was prepared in storage buffer. 6µL of the ligand solution was added to 18µL of the appropriate protein solution in a 384-well plate, and the mixture was allowed to equilibrate at room temperature for 15 min. Polarization measurements were made at 535nm using a Perkin Elmer Victor 3V 1420 plate reader. The resulting anisotropy values were plotted as a function of protein concentration and fit to a single site binding model using the Kaleidagraph software package:

$$FA = \frac{B_{max} * [\mathrm{EP12}]}{K_{D,app} + [\mathrm{EP12}]}$$

Results:

Mapping MamE-dependent cleavage patterns in vivo

To learn more about the context of MamE-dependent proteolysis, we attempted to map the cleavage patterns of MamE, MamP and MamO *in vivo* using an epitope tagging approach. Strains with N- or C-terminally 3xFLAG-tagged alleles of each gene were added to their respective deletion strains. Each of the tagged alleles complemented the biomineralization defects of the deletions with the exception of the C-terminally tagged *mamO* allele (*O-FLAG*). Analysis of cell extracts from these strains by Western blotting was used to assess the processing patterns for each proteolytic target.

For MamE, a number of N-terminal proteolytic fragments but no C-terminal fragments are observed (Fig. 1B), indicating that short segments are sequentially removed from the C-terminus. Interestingly, this seems to culminate in a stable ~45kDa fragment that corresponds to the MamE protease domain and the N-terminal membrane helix separated from the rest of protein. For MamP, one N-terminal band and two C-terminal bands are observed that correspond to a full-length protein and a protein truncated by approximately 10kDa at the N-terminus, indicating the removal of the membrane anchor from the predicted soluble domains (Fig. 1B). For MamO, a full-length and a shorter band are observed for both the N- and C-terminally tagged proteins (Fig. 1B). The pattern predicts that MamE-dependent proteolysis separates the N-terminal protease and C-terminal TauE domains of MamO (Fig. 1A).

In many MamE and MamO blots, there are small (i.e. ~20 kDa) bands near the bottom of the gel when analyzing the N-terminally tagged proteins. Although these bands appear in many experiments, the levels and even the presence of these two signals are inconsistent. This potentially suggests that short segments are removed from the N-terminus of each protein to produce unstable fragments that are quickly degraded. Due to the

inconsistency in these bands we have not focused on them in our analysis of the processing pattern.

Identification of a putative cleavage motif in MamO

Analysis of the *in vivo* processing patterns strongly indicated that MamE processes itself, MamO and MamP(25). We reasoned that one strategy for reconstituting its proteolytic activity *in vitro* could be to design substrates from motifs that are cleaved in a MamE-dependent fashion. Based on epitope tagging, MamO is cleaved between the protease and TauE domains, which suggests that there is a MamE-dependent cleavage site at the mature C-terminus of the protease domain (Fig. 2B). Cell pellets from 2L cultures of the Δ*O*Δ*R9*/*FLAG-O* strain were used for biochemical fractionation. Enzymatic lysis and sonication followed by a low speed (8000 x g) spin were used to isolate material associated with the dense magnetite particles. A number of detergents were tested for their ability to dissolve the MamO fragments. Most classes of detergents are ineffective or only partially effective in the initial solubilization step. Lipid-like zwitterionic detergents including lauryldimethylamine oxide (LDAO) and FosCholine-12 extract the fragments from the membrane, but they disrupt binding to the α-FLAG affinity resin. However, once the initial extraction step is complete, the detergent requirements to maintain solubility become less stringent.

Based on the solubility information, the low speed pellet was pre-washed with CHAPS before extracting the MamO fragments from the membranes with FosCholine-12. In order to facilitate binding to the affinity resin, the FosCholine soluble material was loaded on an anion exchange column and exchanged to the detergent DDM by extensive washing before eluting with salt. This fraction was then used as the input for an α-FLAG affinity isolation to yield a final fraction enriched in N-terminal fragments of MamO (Figs. 2A and 2B).

The concentrated α-FLAG elution was separated on an SDS-PAGE gel, stained with colloidal Coomassie Blue and the region around 35kDa was excised. After performing in-gel trypsin digestion, peptides were extracted and concentrated for LC-MS/MS analysis. A number of peptides from the MamO sequence are consistently detected, and, as expected, they map almost exclusively to the protease domain of MamO (Fig. 2C). In all of the samples, the protein sequence coverage drops off sharply in the linker between the protease and TauE domains (Fig. 2C). A peptide with the sequence GSATAPGQPQTQTV is routinely detected at the C-terminal edge of the peptide coverage (Fig 2D). This peptide results from a predicted tryptic cleavage on the N-terminus but has a non-tryptic C-terminus, which suggests that it contains the C-terminal sequence of the mature MamO protease domain.

Purification of MamE

In order to reconstitute its proteolytic activity *in vitro*, we developed a method to express and purify appreciable amounts of MamE. In the expression construct, the N-terminal membrane anchor is replaced with the OmpA signal peptide to produce a soluble protein that can still undergo heme loading in the periplasm(34). Initial fractionations with an N-terminally 6xHis-tagged form of the protein had significant contamination due to what appeared to be truncated fragments caused by auto-cleavage during expression. To eliminate this problem, a strep tag was added on the C-terminus to allow for a sequential affinity isolation of full-length protein. Finally, MamE has a predicted region of 60-70 disordered residues downstream of the N-terminal membrane anchor and upstream of the trypsin-like domain. Removing this region dramatically improved the solubility.

The expression conditions also had to be carefully optimized in order for MamE to accumulate. Maximum expression occurs with low levels of IPTG induction in C43 cells at 20 °C. The precise details of the expression and purification procedure are described in the Materials and Methods. It allows for the soluble region of MamE as well as a catalytically inactive form ($MamE^{S297A}$) to be purified with yields approaching ~1mg/L. Importantly, both preparations appear red and display absorbance spectra characteristic of *c*-type cytochromes (Fig. 3).

Direct proteolysis of the MamO cleavage motif

We designed a fluorogenic peptide (peptide MamO1) to test as a substrate for purified

MamE. The substrate contains 8 residues that make up the putative cleavage motif identified in MamO (Fig. 2) flanked by an upstream fluorophore and a downstream fluorescence quencher. Normally, the peptide has low fluorescence due to interaction between the fluorophore and quencher. If the peptide is cleaved, the two fragments will separate, resulting in an increase in fluorescence. Upon addition of the O1 peptide to purified MamE, there is a linear increase in fluorescence. Importantly, the $MamE^{S297A}$ protein does not alter the fluorescence indicating the signal is due to serine protease activity from MamE (Fig. 4A). MamE hydrolyzes the O1 peptide with a k_{cat} of 0.64 ± 0.03 min^{-1} and a K_M of 6.1 ± 0.5 μM. As for other HtrA proteases, the reaction is positively cooperative, displaying a Hill coefficient of 1.5 ± 0.1 (Fig. 4B) (19, 35). These values are similar to those reported for cleavage of peptide substrate by other trypsin-like proteases and confirm that MamE can efficiently cleave the motif identified in MamO(36). Combined with the *in vivo* analysis these results confirm that MamO is a direct proteolytic target of MamE.

Reconstitution of MamE auto-proteolysis

Analysis of MamE processing in AMB-1 along with the extensive auto-proteolysis during its expression in *E. coli* suggested that MamE is capable of auto-proteolysis. However, purified MamE is relatively stable such that after an hour of incubation at 30°C, nearly all of the protein remains intact (Fig. 5A). The positive cooperativity observed for the steady-state kinetics of O1 peptide cleavage indicated that MamE's catalytic activity could be stimulated by substrates. This mode of regulation might also lead to peptide-induced activation of auto-cleavage. Indeed, the MamO1 peptide stimulates degradation of full-length MamE in a dose-dependent manner, confirming that MamE's activity can be stimulated by the presence of substrate (Fig. 5A).

Taking advantage of the distinct tags used to purify MamE, we examined the auto-cleavage fragmentation pattern by Western blotting. Numerous truncated proteins are detected by blotting for the N-terminal 6xHis tag, the smallest of which is a ~27 kDa fragment presumed to be the protease domain (Fig. 5B). In contrast, only the full-length protein can be seen when blotting for the C-terminal strep tag (Fig. 5C). The pattern indicates that the reaction proceeds via sequential removal of small fragments from the C-terminus. Furthermore, it matches the pattern seen by examining epitope-tagged alleles of MamE expressed *in vivo* and confirms the successful reconstitution MamE-dependent proteolysis *in vitro.*

Activation through the PDZ domains

PDZ domains of other HtrA proteases regulate proteolytic activity by binding to extended peptide motifs(20). Phage display has been a productive approach for identifying peptide ligands that bind to PDZ domains(37-40). Each of the MamE PDZ domains was purified and used as bait in phage display selections. Both bait proteins showed phage enrichment for specific particles with a library displaying peptides on the N-terminus of the coat protein, but no enrichment was observed in libraries displaying C-terminal fusions. This suggests that, unlike those associated with other HtrA proteases, the MamE PDZ domains do not display a preference for C-terminal peptides(41). Interestingly, phage selections for both domains showed a strong preference for internal regions (Tables 3 and 4). However, a single clone dominated both pools making the identification of consensus motifs hard to interpret.

Peptides corresponding to the sequence that dominated each selection were synthesized and labeled with a fluorescent dye. In addition, the C-terminal region of MamE containing only the PDZ domains (EP12) was purified and used to test for direct binding to the phage-derived ligands. Fluorescence anisotropy experiments demonstrate that both phage-derived peptides bind to the C-terminus of MamE (Fig. 6A). The PDZ1 peptide shows ~10-fold tighter binding than the PDZ2 peptide, but both affinities are comparable to those seen for other PDZ domains(40). Addition of either peptide to full-length MamE, results in a dose-dependent activation of auto-processing (Fig. 6B). Importantly, the activation threshold for the PDZ2 peptide is higher than the PDZ1 peptide, mirroring the equilibrium binding data. These results show that, like other HtrA proteases, MamE's protease activity can be regulated through peptide binding to its PDZ domains.

Misregulation of MamE disrupts biomineralization in vivo

MamE's low basal activity and its stimulation by various peptides define a switch-like behavior that toggles a high activity and a low activity state of the protein. This *in vitro* behavior suggests that modulation of the two states is important during biomineralization *in vivo*. To date, we have not been able to identify growth conditions that prevent *in vivo* processing of MamE, MamO or MamP. Thus, we utilized a genetic approach to examine whether proper regulation of MamE-dependent proteolysis was required for biomineralization.

Work with the model HtrA protease DegS has shown that mutating residue 192 (chymotrypsin numbering) in the oxyanion hole to proline increases basal cleavage rates by shifting the allosteric equilibrium toward the active state (19, 42). We introduced an allele with the corresponding mutation of MamE (Q294P) into the *mamE* null strain (Fig. 7A). This strain displayed significantly less MamE and MamP as assessed by western blotting, indicating increased proteolytic activity from MamE. Additionally, the $mamE^{Q294P}$ allele partially circumvents the requirement for MamO in promoting MamE-dependent proteolysis. MamE and MamP appeared to be processed when the $mamE^{Q294P}$ allele was introduced into a strain lacking both *mamE* and *mamO*, though it did not restore processing of MamE to wild-type levels (Figs. 7B and C). These results indicate that $mamE^{Q294P}$ produces a constitutively active, unregulated protease *in vivo*.

We next examined this allele for its ability to complement the biomineralization defects seen in the *mamE* null strain. While wild-type $mamE^{WT}$ allele completely restores the magnetic response, the $mamE^{Q294P}$ strain has a significantly lower response (Fig. 7D). Thus, both the inactive ($mamE^{PD}$) and constitutively active forms ($mamE^{Q294P}$) of the protease disrupt biomineralization *in vivo*. The magnetic response of the $mamE^{Q294P}$ strain is higher than the negligible signal measured in the $mamE^{PD}$ strain, indicating that the biomineralization process is stalled at a different stage when MamE's activity is unregulated. These results demonstrate that complete biomineralization of magnetosome crystals relies not only on the occurrence of MamE-dependent proteolysis but also careful regulation of the activity.

Discussion

Biochemical principles underlying the biomineralization of magnetite by magnetotactic bacteria represent a model for understanding how biological molecules manipulate inorganic compounds(43). Recent advances describing the genetic basis for this process have paved the way for mechanistic studies of the factors that promote mineral formation(3). The HtrA protease MamE has emerged as a central biomineralization factor in the model organism *Magnetospirillum magneticum* AMB-1. In addition to promoting crystal nucleation and protein localization to the magnetosome, MamE regulates a transition from small superparamagnetic crystals to full-sized paramagnetic particles. This crystal maturation phenotype was linked to MamE's putative protease activity suggesting a model where its catalytic activity controls crystal maturation(14).

Here, we have studied MamE's serine protease activity in detail. We mapped the proteolytic patterns of three *in vivo* targets both at the domain level and, in one case, at the individual residue level. Using this information, we reconstituted a number of aspects of MamE-dependent proteolysis with purified components. We show that MamE directly cleaves a motif from the linker between MamO's protease and TauE domains in a positively cooperative fashion. Furthermore, we show that purified MamE has low basal activity, but that it can be activated in a number of ways including the presence of substrate and peptide binding to either of its PDZ domains. This behavior is consistent with a switch-like mode of regulation in which the protease requires activation by environmental cues. These results also show for the first time that MamE is a serine protease that is capable of degrading itself and other biomineralization factors.

Nearly all studied members of the HtrA family behave as trimers or multiples thereof(16-18, 23, 44, 45). In other systems with two PDZ domains, the first PDZ seems to regulate protease activity directly while the second is thought to mediate rearrangements of core trimers into higher order oligomers(21, 23, 24). Peptide binding to either the first or the second PDZ domain of

MamE can activate proteolysis, although the activation through PDZ2 is much weaker. Furthermore, the protein behaves as a monomer as indicated by gel filtration. Transitions between a monomer and higher order assemblies are rare in the HtrA family, but the positive cooperativity observed for MamE suggests that the active form is indeed a larger assembly(46). The protein production method described here should enable future structural studies aimed at understanding the potential for novel assembly behavior as well as an unusual regulatory role for the second PDZ domain.

The switch like activation of MamE's activity suggested that allosteric regulation of its protease activity was required for proper crystal maturation. Using a mutation reported to stabilize active forms of other HtrA proteases, we showed that, like the catalytically inactive form, a constitutively active form of MamE had defects in crystal maturation(19). These results confirm that both the active and inactive states are important during the process of magnetosome formation. Similar experiments with DegP in *E. coli* indicated that the proper balance between active and inactive forms is required for fitness during heat stress(47). Our results show that, in addition to maintaining fitness during stress, this mode of regulation can be used to control a developmental process.

Taken together, our results are consistent with the checkpoint model for MamE-dependent proteolysis in regulating the maturation of magnetite crystals. However, the detailed mechanism by which that activity promotes crystal growth remains unclear. One possible mechanism could be by controlling the size of the surrounding membrane. A recent study demonstrated a link between the growth of magnetosome membrane compartments and growth of the magnetite crystals within. This finding led to the proposal that there is a checkpoint regulating a second stage of membrane growth after the onset of biomineralization(48). Although *mamE* deletions have intact magnetosome membranes, the sizes of the membranes have not been quantified. It is tempting to speculate that proteolysis controls this switch by linking membrane growth to crystal growth. In this scenario, crystal nucleation in the E^{PD} cells would not lead to membrane growth, while the E^{QP} cells would initiate membrane growth before crystals had grown sufficiently, leading to stunted particles in both cases.

Acknowledgements: This work was supported by grants from the National Institutes of Health (R01GM084122) and the Office of Naval Research (N000141310421) to AK. The QB3/Chemistry Mass Spectrometry Facility at the University of California, Berkeley receives support from the National Institutes of Health (1S10OD020062-01).

Conflict of Interest: The authors declare no conflict of interest.

Author Contributions: DMH coordinated the study, performed majority of experiments and wrote the paper. AK coordinated study, advised on experiments and edited paper. PJB designed and performed experiments on constitutive MamE mutant. ATI advised on and performed mass spectrometry experiments. EHL purified MamE PDZ domains. JT and SSS coordinated and performed phage display experiments to identify peptides that bound to MamE PDZ domains. All authors reviewed the results and approved the final version of the manuscript.

References

1. Blakemore, R. (1975) Magnetotactic Bacteria. *Science*. **190**, 377–379
2. Balkwill, D. L., Maratea, D., and Blakemore, R. P. (1980) Ultrastructure of a magnetotactic spirillum. *J Bacteriol*. **141**, 1399–1408
3. Murat, D., Quinlan, A., Vali, H., and Komeili, A. (2010) Comprehensive genetic dissection of the magnetosome gene island reveals the step-wise assembly of a prokaryotic organelle. *Proc Natl Acad Sci U S A*. **107**, 5593–5598
4. Lohße, A., Ullrich, S., Katzmann, E., Borg, S., Wanner, G., Richter, M., Voigt, B., Schweder, T., and Schüler, D. (2011) Functional Analysis of the Magnetosome Island in Magnetospirillum gryphiswaldense: The mamAB Operon Is Sufficient for Magnetite Biomineralization. *PLoS ONE*. **6**, e25561–10
5. Lohße, A., Borg, S., Raschdorf, O., Kolinko, I., Tompa, E., Posfai, M., Faivre, D., Baumgartner, J., and Schuler, D. (2014) Genetic Dissection of the mamAB and mms6 Operons Reveals a Gene Set Essential for Magnetosome Biogenesis in Magnetospirillum gryphiswaldense. *J Bacteriol*. **196**, 2658–2669
6. Kolinko, I., Lohße, A., Borg, S., Raschdorf, O., Jogler, C., Tu, Q., Pósfai, M., Tompa, É., Plitzko, J. M., Brachmann, A., Wanner, G., Müller, R., Zhang, Y., and Schüler, D. (2014) Biosynthesis of magnetic nanostructures in a foreign organism by transfer of bacterial magnetosome gene clusters. *Nature Nanotechnology*. **9**, 193–197
7. Rahn-Lee, L., Byrne, M. E., Zhang, M., Le Sage, D., Glenn, D. R., Milbourne, T., Walsworth, R. L., Vali, H., and Komeili, A. (2015) A Genetic Strategy for Probing the Functional Diversity of Magnetosome Formation. *PLoS Genet*. **11**, e1004811–18
8. Laura, R. P., Witt, A. S., Held, H. A., Gerstner, R., Deshayes, K., Koehler, M. F. T., Kosik, K. S., Sidhu, S. S., and Lasky, L. A. (2002) The Erbin PDZ Domain Binds with High Affinity and Specificity to the Carboxyl Termini of -Catenin and ARVCF. *J Biol Chem*. **277**, 12906–12914
9. Wolff, A., Frese, K., Wißbrock, M., Eckstädt, K., Ennen, I., Hetaba, W., Löffler, S., Regtmeier, A., Thomas, P., Sewald, N., Schattschneider, P., and Hütten, A. (2012) Influence of the synthetic polypeptide c25-mms6 on cobalt ferrite nanoparticle formation. *J Nanopart Res*. **14**, 1161–11
10. Kashyap, S., Woehl, T. J., Liu, X., Mallapragada, S. K., and Prozorov, T. (2014) Nucleation of Iron Oxide Nanoparticles Mediated by Mms6 Protein in Situ. *ACS Nano*. **8**, 9097–9106
11. Rawlings, A. E., Bramble, J. P., Walker, R., Bain, J., Galloway, J. M., and Staniland, S. S. (2014) Self-assembled MmsF proteinosomes control magnetite nanoparticle formation in vitro. *Proc Natl Acad Sci U S A*. **111**, 16094–16099
12. Yang, W., Li, R., Peng, T., Zhang, Y., Jiang, W., Li, Y., and Li, J. (2010) mamO and mamE genes are essential for magnetosome crystal biomineralization in Magnetospirillum gryphiswaldense MSR-1. *Res Microbiol*. **161**, 701–705
13. Komeili, A., Li, Z., Newman, D. K., and Jensen, G. J. (2006) Magnetosomes Are Cell Membrane Invaginations Organized by the Actin-Like Protein MamK. *Science*. **311**, 242–245
14. Quinlan, A., Murat, D., Vali, H., and Komeili, A. (2011) The HtrA/DegP family protease MamE is a bifunctional protein with roles in magnetosome protein localization and magnetite biomineralization. *Mol Microbiol*. **80**, 1075–1087
15. Clausen, T., Kaiser, M., Huber, R., and Ehrmann, M. (2011) HTRA proteases: regulated proteolysis in protein quality control. *Nat Rev Mol Cell Biol*. **12**, 152–162
16. Krojer, T., Garrido-Franco, M., Huber, R., Ehrmann, M., and Clausen, T. (2002) Crystal structure of DegP (HtrA) reveals a new protease-chaperone machine. *Nature*. **416**, 455–459
17. Wilken, C., Kitzing, K., Kurzbauer, R., Ehrmann, M., and Clausen, T. (2004) Crystal Structure of the DegS Stress Sensor: How a PDZ Domain Recognizes Misfolded Protein and Activates a Protease. *Cell*. **117**, 483–494
18. Li, W., Srinivasula, S. M., Chai, J., Li, P., Wu, J.-W., Zhang, Z., Alnemri, E. S., and Shi, Y. (2002) Structural insights into the pro-apoptotic function of mitochondrial serine protease HtrA2/Omi. *Nat. Struct Biol.* **9**, 436–441

19. Sohn, J., Grant, R. A., and Sauer, R. T. (2010) Allostery Is an Intrinsic Property of the Protease Domain of DegS: IMPLICATIONS FOR ENZYME FUNCTION AND EVOLUTION. *J Biol Chem*. **285**, 34039–34047
20. Krojer, T., Sawa, J., Huber, R., and Clausen, T. (2010) HtrA proteases have a conserved activation mechanism that can be triggered by distinct molecular cues. *Nat Struct Mol Biol*. **17**, 844–852
21. Kim, S., Grant, R. A., and Sauer, R. T. (2011) Covalent Linkage of Distinct Substrate Degrons Controls Assembly and Disassembly of DegP Proteolytic Cages. *Cell*. **145**, 67–78
22. Sohn, J., Grant, R. A., and Sauer, R. T. (2007) Allosteric Activation of DegS, a Stress Sensor PDZ Protease. *Cell*. **131**, 572–583
23. Wrase, R., Scott, H., Hilgenfeld, R., and Hansen, G. (2011) The Legionella HtrA homologue DegQ is aself-compartmentizing protease thatforms large 12-meric assemblies. *Proc Natl Acad Sci U S A*. **108**, 10490–10495
24. Krojer, T., Sawa, J., Schäfer, E., Saibil, H. R., Ehrmann, M., and Clausen, T. (2008) Structural basis for the regulated protease and chaperone function of DegP. *Nature*. **453**, 885–890
25. Hershey, D. M., Ren, X., Melnyk, R. A., Browne, P. J., Ozyamak, E., Jones, S. R., Chang, M. C. Y., Hurley, J. H., and Komeili, A. (2016) MamO Is a Repurposed Serine Protease that Promotes Magnetite Biomineralization through Direct Transition Metal Binding in Magnetotactic Bacteria. *PLoS Biol*. **14**, e1002402
26. Siponen, M. I., Legrand, P., Widdrat, M., Jones, S. R., Zhang, W.-J., Chang, M. C. Y., Faivre, D., Arnoux, P., and Pignol, D. (2014) Structural insight into magnetochrome-mediated magnetite biomineralization. *Nature*. **502**, 681–684
27. Jones, S. R., Wilson, T. D., Brown, M. E., Rahn-Lee, L., Yu, Y., Fredriksen, L. L., Ozyamak, E., Komeili, A., and Chang, M. C. Y. (2015) Genetic and biochemical investigations of the role of MamP in redox control of iron biomineralization in Magnetospirillum magneticum. *Proc Natl Acad Sci U S A*. **112**, 3904–3909
28. Roepstroff, P. (1984) Proposal for a Common Nomenclaturefor Sequence Ions in Mass Spectra of Peptides. *Biomed Mass Spectrom*. **11**, 601
29. Arslan, E., Schulz, H., Zufferey, R., Kunzler, P., and Thony-Meyer, L. (1998) Overproduction of the Bradyrhizobium japonicum c-Type Cytochrome Subunits of the cbb3 Oxidase in Escherichia coli. *Biochemical and Biophysical Research Communications*
30. Held, H. A., and Sidhu, S. S. (2004) Comprehensive Mutational Analysis of the M13 Major Coat Protein: Improved Scaffolds for C-terminal Phage Display. *J Mol Biol*. **340**, 587–597
31. Arita, Y., Allen, S., Chen, G., Zhang, W., Wang, Y., Owen, A. J., Dentinger, P., and Sidhu, S. S. (2016) Rapid isolation of peptidic inhibitors of the solute carrier family transporters OATP1B1 and OATP1B3 by cell-based phage display selections. *Biochemical and Biophysical Research Communications*. 10.1016/j.bbrc.2016.01.050
32. Tonikian, R., Zhang, Y., Boone, C., and Sidhu, S. S. (2007) Identifying specificity profiles for peptide recognition modules from phage-displayed peptide libraries. *Nat Protoc*. **2**, 1368–1386
33. Tonikian, R., Zhang, Y., Sazinsky, S. L., Currell, B., Yeh, J.-H., Reva, B., Held, H. A., Appleton, B. A., Evangelista, M., Wu, Y., Xin, X., Chan, A. C., Seshagiri, S., Lasky, L. A., Sander, C., Boone, C., Bader, G. D., and Sidhu, S. S. (2008) A Specificity Map for the PDZ Domain Family. *PLoS Biol*. **6**, e239–17
34. Londer, Y. Y., Pokkuluri, P. R., Orshonsky, V., Orshonsky, L., and Schiffer, M. (2006) Heterologous expression of dodecaheme "nanowire" cytochromes c from Geobacter sulfurreducens. *Protein Expression and Purification*. **47**, 241–248
35. Mauldin, R. V., and Sauer, R. T. (2012) Allosteric regulation of DegS protease subunits through a shared energy landscape. *Nature Chemical Biology*. **9**, 90–96
36. Small, J. L., O'Donoghue, A. J., Boritsch, E. C., Tsodikov, O. V., Knudsen, G. M., Vandal, O., Craik, C. S., and Ehrt, S. (2013) Substrate Specificity of MarP, a Periplasmic Protease Required for Resistance to Acid and Oxidative Stress in Mycobacterium tuberculosis. *J Biol Chem*. **288**, 12489–12499

37. Fuh, G., Pisabarro, M. T., Li, Y., Quan, C., Lasky, L. A., and Sidhu, S. S. (2000) Analysis of PDZ Domain-Ligand Interactions Using Carboxyl-terminal Phage Display. *J Biol Chem*. **275**, 21486–21491
38. Zhang, Y., Appleton, B. A., Wu, P., Wiesmann, C., and Sidhu, S. S. (2007) Structural and functional analysis of the ligand specificity of the HtrA2/Omi PDZ domain. *Protein Sci.* **16**, 1738–1750
39. Runyon, S. T., Zhang, Y., Appleton, B. A., Sazinsky, S. L., Wu, P., Pan, B., Wiesmann, C., Skelton, N. J., and Sidhu, S. S. (2007) Structural and functional analysis of the PDZ domains of human HtrA1 and HtrA3. *Protein Sci.* **16**, 2454–2471
40. Ivarsson, Y., Arnold, R., McLaughlin, M., Nim, S., Joshi, R., Ray, D., Liu, B., Teyra, J., Pawson, T., Moffat, J., Li, S. S. C., Sidhu, S. S., and Kim, P. M. (2014) Large-scale interaction profiling of PDZ domains through proteomic peptide-phage display using human and viral phage peptidomes. *Proc Natl Acad Sci U S A*. **111**, 2542–2547
41. Lee, H.-J., and Zheng, J. J. (2010) PDZ domains and their binding partners: structure, specificity, and modification. *Cell Commun Signal*. **8**, 8–18
42. Perona, J. J., and Craik, C. S. (1997) Evolutionary Divergence of Substrate Specificity within the Chymotrypsin-like Serine Protease Fold. *J Biol Chem*. **272**, 29987–29990
43. Komeili, A. (2011) Molecular mechanisms of compartmentalization and biomineralization in magnetotactic bacteria. *FEMS Microbiology Reviews*. **36**, 232–255
44. MohamedMohaideen, N. N., Palaninathan, S. K., Morin, P. M., Williams, B. J., Braunstein, M., Tichy, S. E., Locker, J., Russell, D. H., Jacobs, W. R., and Sacchettini, J. C. (2008) Structure and Function of the Virulence-Associated High-Temperature Requirement A of Mycobacterium tuberculosis. *Biochemistry*. **47**, 6092–6102
45. Truebestein, L., Tennstaedt, A., Mönig, T., Krojer, T., Canellas, F., Kaiser, M., Clausen, T., and Ehrmann, M. (2011) Substrate-induced remodeling of the active site regulates human HTRA1 activity. *Nat Rev Mol Cell Biol*. **18**, 386–388
46. Kley, J., Schmidt, B., Boyanov, B., Stolt-Bergner, P. C., Kirk, R., Ehrmann, M., Knopf, R. R., Naveh, L., Adam, Z., and Clausen, T. (2011) Structural adaptation of the plant protease Deg1 to repair photosystem II during light exposure. *Nat Rev Mol Cell Biol*. **18**, 728–731
47. Kim, S., and Sauer, R. T. (2014) Distinct regulatory mechanisms balance DegP proteolysis to maintain cellular fitness during heat stress. *Genes & Development*. **28**, 902–911
48. Cornejo, E., Subramanian, P., Li, Z., Jensen, G. J., and Komeili, A. (2016) Dynamic Remodeling of the Magnetosome Membrane Is Triggered by the Initiation of Biomineralization. *mBio*. **7**, e01898–15–9

FIGURE LEGENDS

FIGURE 1. *In vivo* proteolytic processing of MamE, MamP and MamO. *A,* Predicted domain structures of the three proteolytic targets. Grey cylinder: transmembrane helix; blue: trypsin-like domain; red: *c*-type cytochrome; yellow: PDZ domain; green: TauE domain. *B,* Proteolytic processing patterns observed through epitope tagging. The inferred sizes of each fragment are indicated. The fragments were observed in each of at least four independent experiments with the exception of the 20kDa N-terminal fragment of MamE and the 17kDa N-terminal fragment of MamO, which varied dramatically between experiments.

FIGURE 2. Biochemical fractionation to enrich N-terminal MamO fragments. *A,* Schematic of the enrichment procedure. *B,* Western blot of each fraction from *A*. The predicted protease domain fragment in marked with a red box. *C,* Peptides identified in a representative LC-MS/MS analysis. The red letters in the MamO sequence represent predicted tryptic cleavage sites. The coverage pattern is characteristic of analyses for three separate preparations. *D,* Tandem mass spectrum from collision-induced dissociation of the $[M+2H]^{2+}$ ion of the peptide, GSATAPGQPQTQTV, corresponding to amino acid residues 273-286 of MamO. The inset shows detail for the isotopically resolved, unfragmented peptide precursor ion. The fragment ion at $m/z = 663$ (denoted by the asterisk) is due to precursor ion that has undergone neutral loss of a molecule of water. This peptide was detected in each of three biological replicate experiments.

FIGURE 3. Purification of MamE. *A,* MamE and $MamE^{S297A}$ (residues 108-728) were purified as a fusion to an N-terminal 6xHis and C-terminal strep tag. *B,* Absorbance spectrum of $MamE^{S297A}$ in the oxidized (blue) and dithionite reduced (red) forms.

FIGURE 4. Cleavage of the MamO1 fluorogenic substrate. *A,* Linear increase in fluorescence upon addition of 20μM MamO1 peptide to 200nM MamE (black circles). No increase is seen with peptide addition to $MamE^{S297A}$ (white circles). *B,* Steady-state kinetics of O1 cleavage by MamE. The dotted line represents a fit to the Hill form of the Michelis-Menten equation. Error bars represent the standard deviation from three technical replicates. The plot is characteristic of the data seen in five biological replicates.

FIGURE 5. Reconstitution of MamE auto-processing. *A,* The MamO1 substrate induces auto-cleavage of MamE. The processing pattern was assessed by Western blots (*B* and *C)* of the reaction containing 320μM O1 for the indicated tag on MamE. The experiment is representative of three biological replicates.

FIGURE 6. Peptide binding to the PDZ domains activates MamE. *A,* Fluorescence anisotropy showing binding of the EPDZ1* peptide to the EP12 protein. The error bars represent the standard deviation from three technical replicates. The dotted line represents a fit of the data to a single-site binding model. *B,* Binding of the EPDZ2* peptide to the EP12 protein. *C,* Activation of MamE auto-cleavage by the EPDZ1* peptide. *D,* Activation of MamE auto-cleavage by the EPDZ2* peptide. Each experiment was repeated a minimum of three times.

FIGURE 7. A constitutively active form of MamE disrupts biomineralization. *A,* Alignment of HtrA proteases. The red star marks position 192 in the oxyanion hole (residue 198 in DegS), and the blue star marks the catalytic serine nucleophile. *B* and *C,* Immunoblot analysis of AMB-1 lysates probed for MamE (*B*) and MamP (*C*). Circles mark full-length proteins and carats mark proteolytic fragments. NS marks nonspecific bands reacting with each antibody preparation. *D,* Magnetic response of AMB-1 cultures with the indicated genetic background. Biological replicates represent independent cultures of each strain and each measurement represents the average and standard deviation from three independent experiments.

TABLE 1. Strains used in this study.

TABLE 2. Plasmids used in this study.

TABLE 3. Peptide sequences from the phage display selections using MamE PDZ1. The sequences are aligned based on the motif **ψ**xxx**Ω**, where ψ is a hydrophilic residue and Ω is an aromatic residue. Bold type is used to mark the hydrophilic and aromatic residues around which the sequences were aligned.

TABLE 4. Peptide sequences from the phage display selections using MamE PDZ2. The sequences are aligned based on the motif ψΦ**G**ΦΦΦ, where ψ is a hydrophobic residue and Φ is a hydrophilic residue. Bold type is used to mark the glycine residue around which the sequences were aligned.

Table 1

Strain	Organism	Description	Source
AK30	*M. magneticum* AMB-1	Wild-type AMB-1	(3)
AK69	*M. magneticum* AMB-1	Δ*mamP*	(3)
AK96	*M. magneticum* AMB-1	Δ*mamE* Δ*limE*	(14)
AK94	*M. magneticum* AMB-1	Δ*mamO* Δ*R9*	(14)
AK205	*M. magneticum* AMB-1	Δ*mamE* Δ*mamO* Δ*R9*	(25)
C43	*E. coli*	protein expression strain	Lucigen
BL21 CodonPlus	*E. coli*	protein expression strain; Cm^R	Agilent
DH5α (*λpir*)	*E. coli*	standard cloning strain	(3)
WM3064	*E. coli*	mating strain; DAP auxotroph used for plasmid transfer	(3)

Table 2

Plasmid	Description	Source
pAK605	Plasmid for expressing protein under control of the *mamH* promoter; non-replicative in AMB-1: integrates upstream of amb0397	(25)
pAK701	pAK605 containing N-terminally 3xFLAG tagged *mamE*	This work
pAK702	pAK605 containing C-terminally 3xFLAG tagged *mamE*	This work
pAK787	pAK605 containing N-terminally 3xFLAG tagged *mamP*	This work
pAK788	pAK605 containing C-terminally 3xFLAG tagged *mamP*	This work
pAK823	pAK605 containing N-terminally 3xFLAG tagged *mamO*	(25)
pAK1003	pAK605 containing C-terminally 3xFLAG tagged *mamO*	This work
pAK1005	pLBM4; LIC compatible vector for expressing fusions to the OmpA signal peptide under the control of the *lac* promoter	(34)
pAK1004	pEC86; plasmid constitutively expressing the *E. coli ccm* genes for *c*-type cytochrome maturation	(29)
pAK825	pLBM4 containing 6xHis-TEV-MamE(resi 108-728)-strep fused to the OmpA signal peptide	This work
pAK964	pAK825 with the S297A mutation in MamE	This work
pAK619	pAK605 containing *mamE*	(25)
pAK620	pAK605 containing $mamE^{PD}$ (H188A T211A S297A mutant)	(25)
pAK999	pAK605 containing $mamE^{QP}$ (Q294P mutant)	This work
pAK1000	pET based vector expressing the first PDZ domain of MamE (resi 489-588) fused to 6xHis-MBP-TEV at the N-terminus	This work
pAK1001	pET based vector expressing the second PDZ domain of MamE (resi 634-728) fused to 6xHis-MBP-TEV at the N-terminus	This work
pAK1002	pET based vector expressing the first and second PDZ domains of MamE (resi 489-728) fused to 6xHis-MBP-TEV at the N-terminus	This work

Table 3

Peptide Sequence																						Count
-	-	W	S	Q	E	M	**E**	D	W	F	**W**	Q	M	P	L	S	G	-	-	-	-	37
-	-	-	-	-	-	F	**N**	Y	E	Q	**W**	L	Q	A	E	Y	L	Q	E	H	-	3
-	-	-	-	-	D	D	**E**	W	W	M	**W**	V	E	Q	K	L	H	E	A	T	-	2
-	-	-	-	P	E	T	**Q**	Y	W	L	**W**	L	M	E	L	D	S	Q	G	-	-	2
M	L	Y	N	F	F	E	**Q**	G	W	W	**W**	Y	F	S	W	-	-	-	-	-	-	2
E	D	Q	S	K	L	D	**Q**	Y	S	K	**W**	M	L	M	L	-	-	-	-	-	-	1
-	-	I	D	T	L	V	**E**	H	H	W	**W**	G	T	V	T	T	F	-	-	-	-	1
-	-	-	-	-	-	P	**E**	F	D	E	**W**	F	E	Q	R	Y	E	E	M	E	K	1
-	-	-	-	-	V	F	**D**	Y	W	Q	**W**	V	M	E	D	T	D	G	M	I	-	1
-	-	W	E	W	P	D	**D**	A	W	Q	**F**	L	T	R	M	S	T	-	-	-	-	1
-	-	-	-	-	-	F	**D**	Y	W	E	**Y**	I	S	H	A	E	Q	P	S	D	L	1

Table 4

Peptide Sequence	Count
- - - - - - - - - M E D Y **G** I F M T S P E G P W A	22
- G Q I E P T W M W D M Y **G** F K L - - - - - - - -	2
S Y V P G E W Q G L E S M **G** I V M - - - - - - - -	2
- A Q E A D Y P A L Y Q L **G** F I P - - - - - - - -	1
- - E H W Q D Y S F E S L **G** I Y I - - - - - - - -	1
- E S P V E W D Y L E S F **G** L V I - - - - - - - -	1
- - - - - - E W S F Q D M **G** F M L S Y D Q M G - -	1
- - - - I A P D L W Y N W **G** I M W R D G - - - - -	1
- - I S Q E P L Y I E Q L **G** M M V F - - - - - - -	1
- - - - - - N E M D N L M **G** M I F M S P E - - -	1
- - - - - - N H A Y Q D F **G** F V V S E L Q E - - -	1
- - P F M P L E Y W Q F M **G** I V F T - - - - - - -	1
- - - - P G T F E D A T L **G** F T W F H D - - - - -	1
- Q N N Q D M M F Q P E L **G** I W F - - - - - - - -	1
- - - - R M P E S M R D M **G** F S I L M A - - - - -	1
- - - - - - Y H G V N E L **G** L M M M D Y I P - - -	1

Figure 1

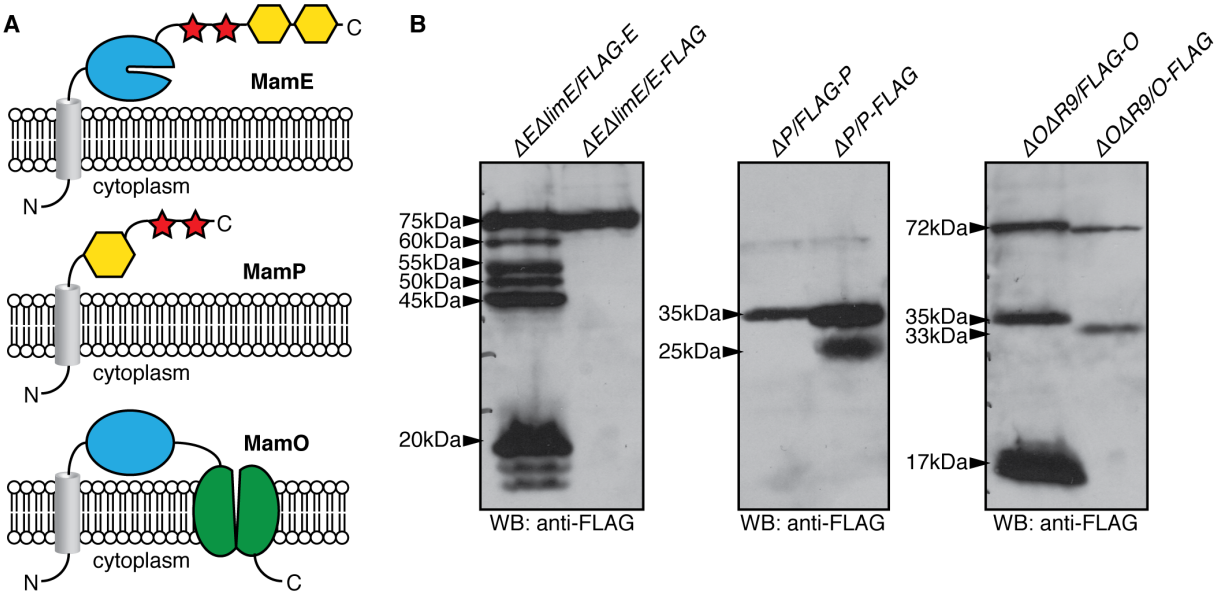
A
C
MamE
cytoplasm
N
C
MamP
cytoplasm
N
MamO
cytoplasm
N
C
B
ΔEΔlimE/FLAG-E
ΔEΔlimE/E-FLAG
75kDa
60kDa
55kDa
50kDa
45kDa
20kDa
WB: anti-FLAG
ΔP/FLAG-P
ΔP/P-FLAG
35kDa
25kDa
WB: anti-FLAG
ΔOΔR9/FLAG-O
ΔOΔR9/O-FLAG
72kDa
35kDa
33kDa
17kDa
WB: anti-FLAG

Figure 2

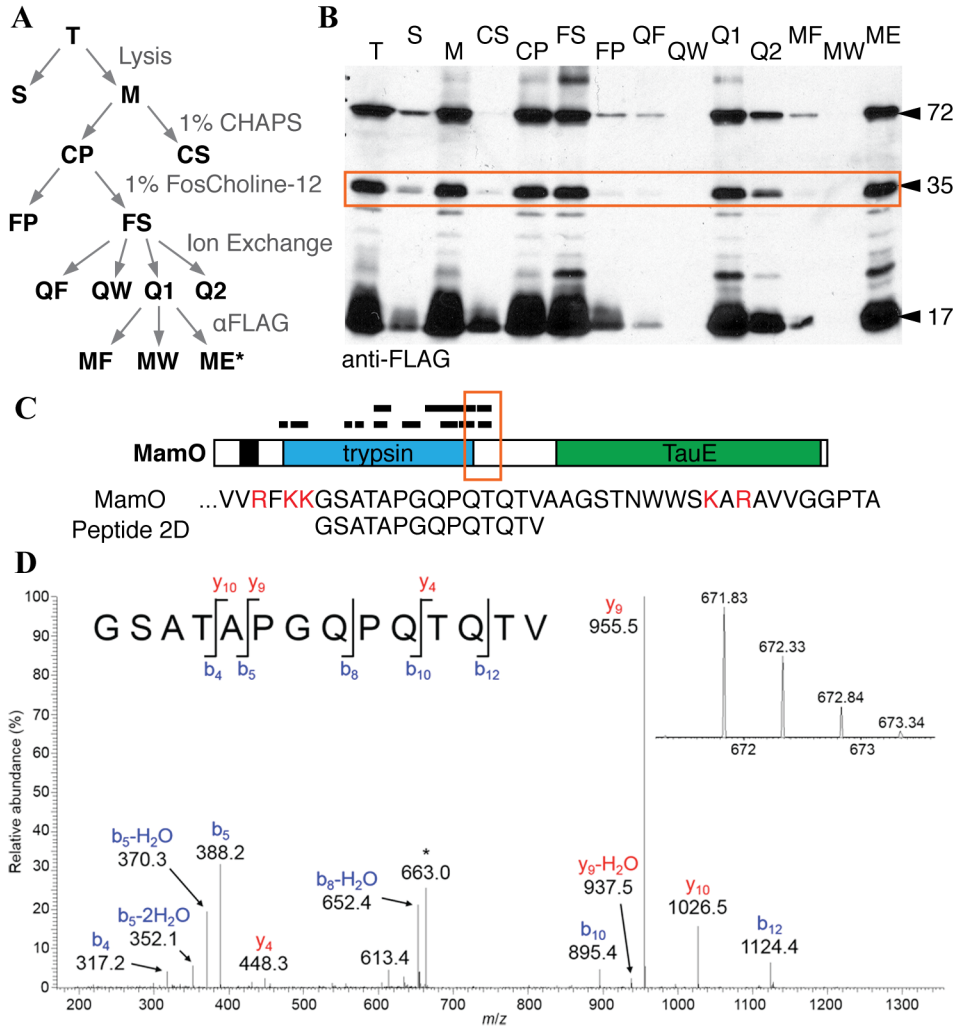
A
T
Lysis
S
M
1% CHAPS
CP
CS
1% FosCholine-12
FP
FS
Ion Exchange
QF
QW
Q1
Q2
αFLAG
MF
MW
ME*
B
T S M CS CP FS FP QF QW Q1 Q2 MF MW ME
72
35
17
anti-FLAG
C
MamO
trypsin
TauE
MamO ...VVRFKKGSATAPGQPQTQTVAAGSTNWWSKARAVVGGPTA
Peptide 2D GSATAPGQPQTQTV
D
G S A T A P G Q P Q T Q T V
y10 y9 y4
b4 b5 b8 b10 b12
y9 955.5
671.83
672.33
672.84
673.34
672
673
b5-H2O 370.3
b5 388.2
b5-2H2O 352.1
b4 317.2
y4 448.3
613.4
b8-H2O 652.4
663.0
y9-H2O 937.5
b10 895.4
y10 1026.5
b12 1124.4
Relative abundance (%)
m/z

Figure 3

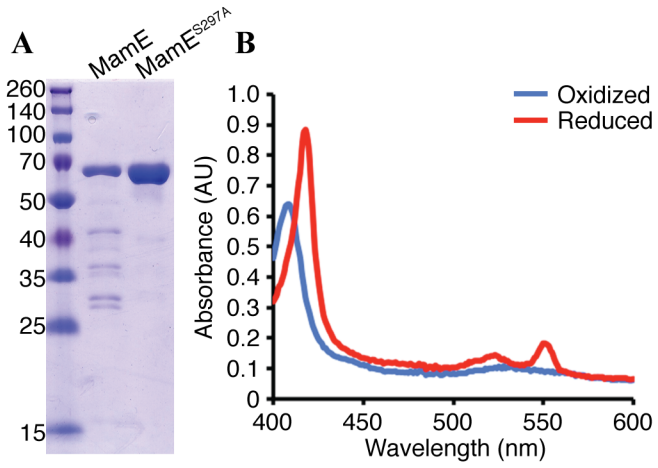
A
MamE
MamE^S297A
260
140
100
70
50
40
35
25
15
B
Oxidized
Reduced
Absorbance (AU)
1.0
0.9
0.8
0.7
0.6
0.5
0.4
0.3
0.2
0.1
0
400
450
500
550
600
Wavelength (nm)

Figure 4

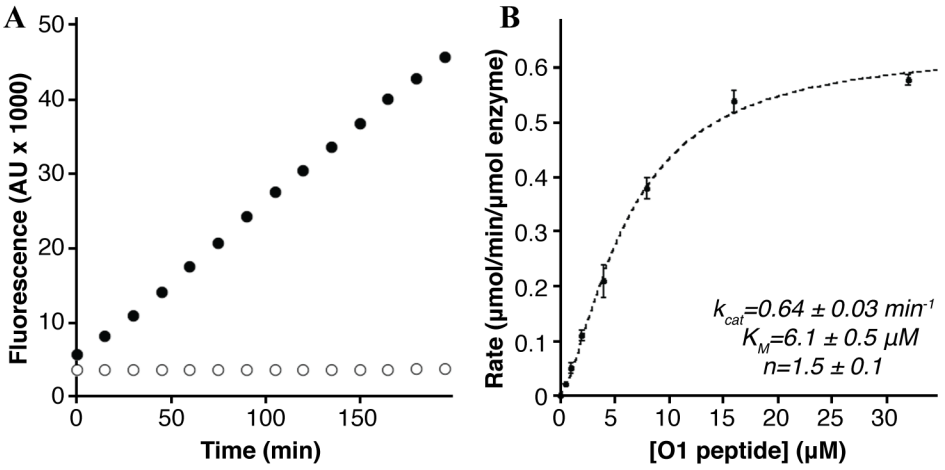
A
Fluorescence (AU x 1000)
Time (min)
B
Rate (µmol/min/µmol enzyme)
[O1 peptide] (µM)
k_{cat}=0.64 ± 0.03 min^{-1}
K_M=6.1 ± 0.5 µM
n=1.5 ± 0.1

Figure 5

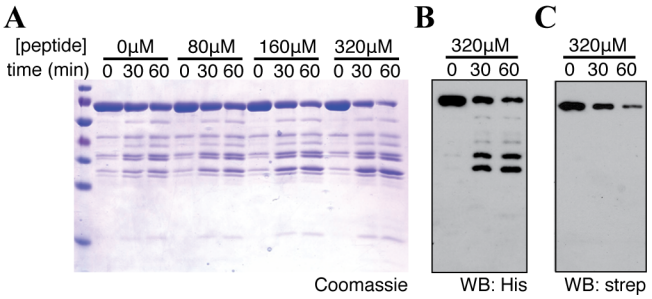
A
B
C
[peptide]
0μM
80μM
160μM
320μM
time (min)
0 30 60 0 30 60 0 30 60 0 30 60
320μM
0 30 60
320μM
0 30 60
Coomassie
WB: His
WB: strep

Figure 6

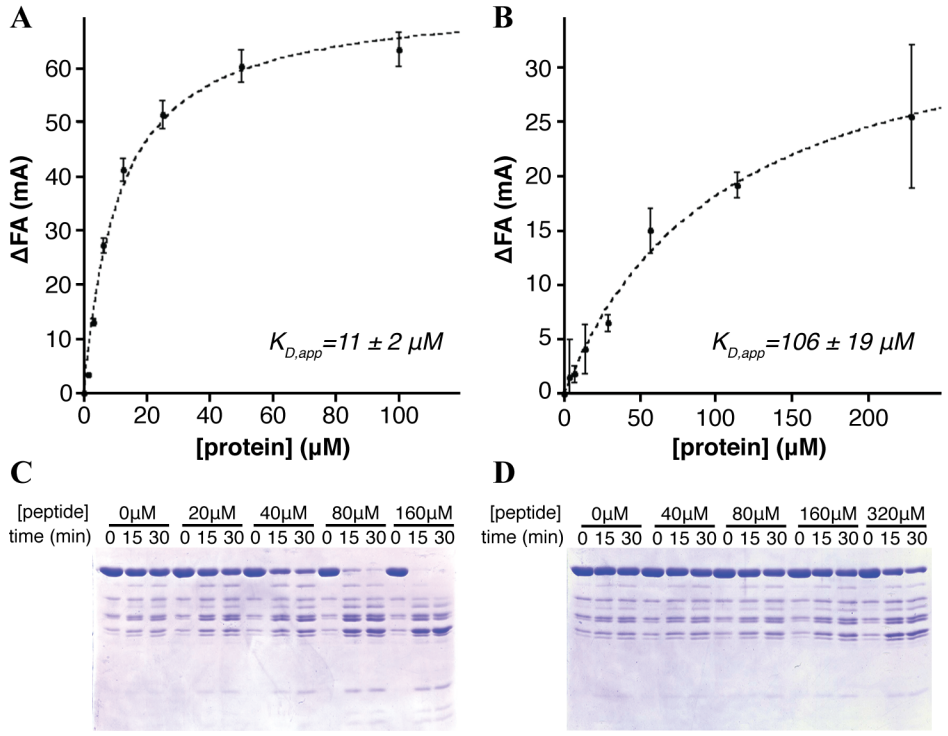
A
ΔFA (mA)
[protein] (μM)
$K_{D,app}$=11 ± 2 μM
B
ΔFA (mA)
[protein] (μM)
$K_{D,app}$=106 ± 19 μM
C
[peptide] 0μM 20μM 40μM 80μM 160μM
time (min) 0 15 30 0 15 30 0 15 30 0 15 30 0 15 30
D
[peptide] 0μM 40μM 80μM 160μM 320μM
time (min) 0 15 30 0 15 30 0 15 30 0 15 30 0 15 30

Figure 7

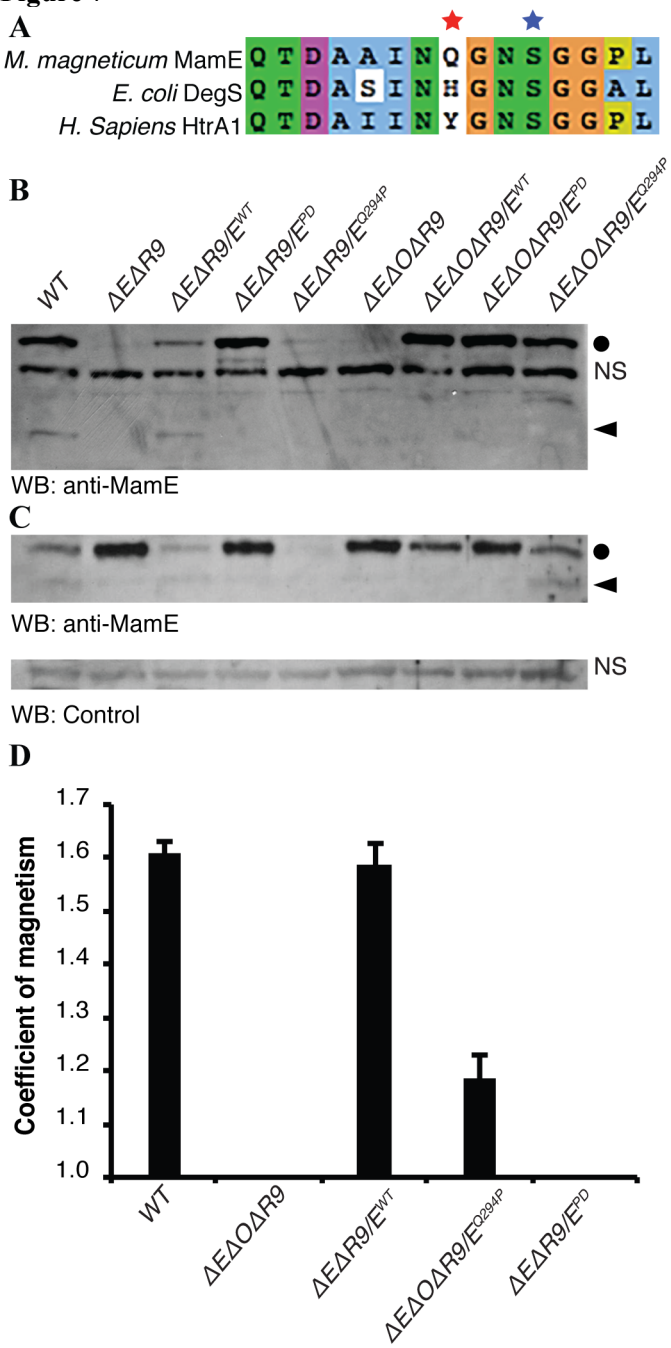
A
M. magneticum MamE Q T D A A I N Q G N S G G P L
E. coli DegS Q T D A S I N H G N S G G A L
H. Sapiens HtrA1 Q T D A I I N Y G N S G G P L
B
WT
ΔEΔR9
ΔEΔR9/E^WT
ΔEΔR9/E^PD
ΔEΔR9/E^Q294P
ΔEΔOΔR9
ΔEΔOΔR9/E^WT
ΔEΔOΔR9/E^PD
ΔEΔOΔR9/E^Q294P
NS
WB: anti-MamE
C
WB: anti-MamE
NS
WB: Control
D
Coefficient of magnetism
1.7
1.6
1.5
1.4
1.3
1.2
1.1
1.0
WT
ΔEΔOΔR9
ΔEΔR9/E^WT
ΔEΔOΔR9/E^Q294P
ΔEΔR9/E^PD